

Precision measurement of the environmental temperature by tunable double optomechanically induced transparency with a squeezed field

Qiong Wang^{1,2}, Jian-Qi Zhang^{1,*}, Peng-Cheng Ma^{1,3}, Chun-Mei Yao², and Mang Feng^{1†}

¹ *State Key Laboratory of Magnetic Resonance and Atomic and Molecular Physics,*

Wuhan Institute of Physics and Mathematics, Chinese Academy of Sciences, Wuhan 430071, China

² *College of Physics and Electronics, Hunan University of Arts and Science, Changde 415000, China and*

³ *School of Physics and Electronic Electrical Engineering, Huaiyin Normal University, Huaian, 223300, China*

A tunable double optomechanically induced transparency (OMIT) with a squeezed field is investigated in a system consisting of an optomechanical cavity coupled to a charged nanomechanical resonator via Coulomb interaction. Such a double OMIT can be achieved by adjusting the strength of the Coulomb interaction, and observed even with a single-photon squeezed field at finite temperature. Since it is robust against the cavity decay, but very sensitive to some parameters, such as the environmental temperature, the model under our consideration can be applied as a quantum thermometer for precision measurement of the environmental temperature within the reach of current techniques.

PACS numbers: 42.50.Wk, 46.80.+j, 41.20.Cv

I. INTRODUCTION

Electromagnetically induced transparency (EIT) is a kind of effect with a narrow transparency window within an absorption line of atoms [1], due to quantum interference between two quantum pathways in Λ -type atoms. This effect plays a key role in modern quantum optics experiments and applications, such as enhanced nonlinear susceptibility [2], optical switch [3], slow and fast lights [4], quantum memory [5–7], quantum interference [8] and vibrational cooling [9]. Recently, the study of the EIT has been extended to multi-channels, e.g., the double EIT [10, 11], and focused on simulation of other physical phenomena, including Anderson localization [12] and quasi-charged particles [13].

The EIT analog occurring in an optomechanical system is called optomechanically induced transparency (OMIT) [14], which is caused by quantum interference between two quantum channels in a Λ -type hybrid level configuration composed of photon states of the cavity and phonon states of the optomechanical resonator [15, 16]. The OMIT has been explored both theoretically [17] and experimentally [14, 18–20]. Similar to the EIT, the study of the originally defined OMIT [21] was extended to the double OMIT by two coupled optomechanical resonators [22] or by an optomechanical resonator coupled to other systems [23, 24]. Besides, the double OMIT was explored from the fixed double OMIT [22, 23, 25] to the tunable one involving a controllable coupling [24].

The present paper intends to investigate the unique behavior of a double OMIT with a squeezed field. Due to involvement of the squeezed field, the OMIT is robust against quantum noise and thus possible to be a

candidate of quantum memory [26]. But if the model is extended to be a double OMIT in a tunable manner, the physics turns to be largely different. The key point is that the double OMIT is robust to the cavity decay and quantum noise of the environment can be correlated to the temperature-dependent noise. As such, we may carry out precision measurement of the environmental temperature, assisted by the squeezed field and the homodyne spectroscopy. Using other unique characteristics, precision measurements of other parameters of the system are also available. This implies that the model under our consideration is by no means a simple extension of the previously considered OMIT [26], but with much different characteristics and applications.

The temperature dependence is from the quantum field involved in our double OMIT, by which we are able to know the environmental temperature through detecting the noise spectra of the optomechanics [27]. This is very different from the OMIT with classical lights [14, 24, 28], whose noise spectra have no relevance to the environmental temperature even under the cryogenic condition [14]. In this context, our scheme is also very different from the previous OMIT measurements resulted from the properties of the OMIT spectra [21, 24]. As a result, our scheme provides a new paradigm for precision measurement based on the noise [29, 30]. On the other hand, compared with the conventional OMIT [26], our double OMIT characterizes as a linear variation of the peak value with respect to the environmental temperature, which is robust to the cavity decay and does not vary with the Coulomb coupling between the two nano-mechanical resonators (NAMRs). This feature exists no matter whether the two NAMRs are identical or not, which is useful for practical applications as discussed later.

The paper is organized as follows. In Sec. II, we present the solution to the model of our designed double OMIT and focus on the spectra via a homodyne detection. In Sec. III, some calculations are made nu-

*Electronic address: Changjianqi@gmail.com

†Electronic address: mangfeng@wipm.ac.cn

merically with experimentally available values, justifying some unique features, such as robustness against the cavity decay and invariance with the Coulomb coupling strength. The feasibility of precision measurement of the environmental temperature is discussed in Sec. IV. Other extended discussion is made in Sec.V and a brief conclusion is given in the last section.

II. THE MODEL AND SOLUTION

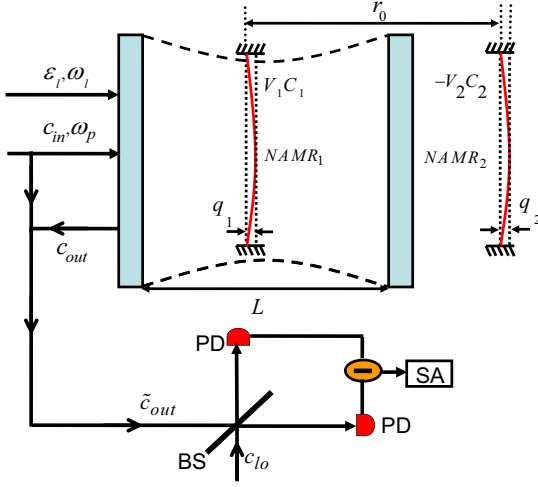


FIG. 1: (Color online) Schematic diagram of the double OMIT system and the measurement. A high-quality Fabry-Perot cavity consists of two fixed mirrors and a charged NAMR₁, which is charged by the bias gate voltage V_1 and subject to the Coulomb force due to the charged NAMR₂ outside the cavity and with the bias gate voltage V_2 . The optomechanical cavity of length L is driven by two light fields, one of which is the pump field ε_l with frequency ω_l and the other of which is the probe field c_{in} with frequency ω_p . q_1 and q_2 represent, respectively, the small displacements of the two NAMRs from their equilibrium positions, with r_0 the equilibrium distance between them. The output field c_{out} from the cavity turns to be \tilde{c}_{out} , which is mixed with a strong local field c_{lo} centered around the probe frequency ω_p at a 50:50 beam splitter (BS). Finally the homodyne spectra are obtained by the spectrum analyzer (SA) assisted by two photon detectors (PD).

As sketched in Fig. 1, there are two charged NAMRs with one (NAMR₁) inside a Fabry-Perot (FP) cavity coupling to the cavity mode by the radiation pressure and interacting with the other (NAMR₂) outside the cavity. The FP cavity contains two mirrors distant by L with the left-hand side mirror partially transmitting and the right-hand side one 100% reflecting. There is a driving on the cavity mode from the left-hand side mirror by a strong coupling field with frequency ω_l . The system can

be described as

$$H_{whole} = \hbar\omega_c c^\dagger c + \sum_{j=1}^2 \left(\frac{p_j^2}{2m_j} + \frac{1}{2} m_j \omega_j^2 q_j^2 \right) - \hbar g c^\dagger c q_1 + H_I + i\hbar\varepsilon_l (c^\dagger e^{-i\omega_l t} - H.C.), \quad (1)$$

where the first term is for the single-mode cavity field with frequency ω_c and annihilation (creation) operator $c(c^\dagger)$. The second and third terms describe the vibration of the charged NAMRs with frequency $\omega_1(\omega_2)$ and effective mass $m_1(m_2)$. $p_1(p_2)$ and $q_1(q_2)$ are the momentum and the position operators of NAMR₁ (NAMR₂), respectively. The fourth term presents the radiation pressure coupling the cavity field to the NAMR₁ with a coupling strength $g = \omega_c/L$.

Coulomb coupling between the two charged NAMRs is given by $H_I = \frac{-C_1 V_1 C_2 V_2}{4\pi\varepsilon_0 |r_0 + q_1 - q_2|}$, where r_0 is the distance between the equilibrium positions, and NAMR₁ and NAMR₂ take the charges $C_1 V_1$ and $-C_2 V_2$ with C_1 and C_2 being the capacitance of the gates, respectively. Under the assumption that the deformations of the NAMRs are much less than their distance ($q_1, q_2 \ll r_0$), the Hamiltonian H_I can be expanded to the second order as $H_I = \frac{-C_1 V_1 C_2 V_2}{4\pi\varepsilon_0 r_0} \left[1 - \frac{q_1 - q_2}{r_0} + \frac{(q_1 - q_2)^2}{r_0^2} \right]$. Since the linear term may be absorbed into the definition of the equilibrium positions, and the quadratic term includes the renormalized oscillation frequencies for both the NAMRs, we have a reduced form $H_I = \hbar\lambda q_1 q_2$ for $\lambda = \frac{C_1 V_1 C_2 V_2}{2\pi\hbar\varepsilon_0 r_0^3}$ [31, 32].

The last term represents the cavity field driven by an input field with frequency ω_l , where the pump field strength $\varepsilon_l = \sqrt{2\kappa\varphi/\omega_l}$ depends on the power φ of the coupling field and the cavity decay rate κ .

In a frame rotating with the pump field frequency ω_l , the Hamiltonian in Eq. (1) is rewritten as

$$H_{total} = \hbar\Delta_c c^\dagger c + \sum_{j=1}^2 \left(\frac{p_j^2}{2m_j} + \frac{1}{2} m_j \omega_j^2 q_j^2 \right) - \hbar g c^\dagger c q_1 + \hbar\lambda q_1 q_2 + i\hbar\varepsilon_l (c^\dagger - c), \quad (2)$$

with $\Delta_c = \omega_c - \omega_l$. Considering the decay rates γ_1 and γ_2 for the NAMR₁ and NAMR₂, respectively, we obtain the corresponding frequency-domain correlation functions for the thermal noise ξ_1 and ξ_2 at a temperature T ,

$$\langle \xi_\tau(\omega) \xi_\tau(\Omega) \rangle = 2\pi\hbar\gamma_\tau m_\tau \omega \left[1 + \coth \left(\frac{\hbar\omega}{2k_B T} \right) \right] \delta(\omega + \Omega),$$

where $\tau = 1, 2$ and k_B is the Boltzmann constant.

We assume that the cavity mode c couples to the input quantum field c_{in} , which is a narrow-band squeezed field with the center around the frequency $\omega_p = \omega_c + \omega_l$ and with a finite bandwidth Γ . The nonvanishing correlation functions for this input squeezed field are given by

$$\langle c_{in}(\omega) c_{in}(\Omega) \rangle = 2\pi \frac{M\Gamma^2}{\Gamma^2 + (\omega - \omega_1)^2} \delta(\omega + \Omega - 2\omega_1),$$

$$\langle c_{in}(\omega)c_{in}^\dagger(-\Omega) \rangle = 2\pi \left[\frac{N\Gamma^2}{\Gamma^2 + (\omega - \omega_1)^2} + 1 \right] \delta(\omega + \Omega), \quad (3)$$

where N is the photon number in the squeezed vacuum, and $M = \sqrt{N(N+1)}$ is an anti-normally ordered term including a broadband contribution from the vacuum noise.

Considering the input squeezed field, Eq. (2) under dissipation and fluctuation is governed by quantum Langevin equations, yielding

$$\begin{aligned} \dot{q}_1 &= \frac{p_1}{m_1}, & \dot{q}_2 &= \frac{p_2}{m_2}, \\ \dot{c} &= -[\kappa + i(\Delta_c - gq_1)]c + \varepsilon_l + \sqrt{2\kappa}c_{in}, \\ \dot{p}_1 &= -m_1\omega_1^2 q_1 - \hbar\lambda q_2 + \hbar g c^\dagger c - \gamma_1 p_1 + \xi_1, \\ \dot{p}_2 &= -m_2\omega_2^2 q_2 - \hbar\lambda q_1 - \gamma_2 p_2 + \xi_2, \end{aligned} \quad (4)$$

whose steady solutions are given by,

$$p_{1s} = p_{2s} = 0, \quad q_{1s} = \frac{\hbar g |c_s|^2}{m_1 \omega_1^2 - \frac{\hbar^2 \lambda^2}{m_2 \omega_2^2}},$$

$$q_{2s} = \frac{\hbar \lambda q_{1s}}{-m_2 \omega_2^2}, \quad c_s = \frac{\varepsilon_l}{\kappa + i\Delta}, \quad (5)$$

with $\Delta = \Delta_c - gq_{1s}$ being the effective detuning between the cavity and the driven fields.

Next, we consider the linear operators as steady mean values plus additional fluctuation operators,

$$q_\tau = q_{\tau s} + \delta q_\tau, \quad p_\tau = p_{\tau s} + \delta p_\tau, \quad c = c_s + \delta c,$$

where $\delta q_\tau, \delta p_\tau, \delta c$ are small fluctuations around the corresponding steady values. Since the steady values have no contribute on the output fields, we only focus on the fluctuation operators, which work as the probe fields and influence the output fields.

Defining the fluctuation operators $\mathbf{X} = (\delta p_1(\omega), \delta q_1(\omega), \delta p_2(\omega), \delta q_2(\omega), \delta c(\omega), \delta c^\dagger(\omega))^T$, we reach the linearized quantum Langevin equations $\mathbf{A}\mathbf{X} = \mathbf{B}$ for the fluctuation operators from Eq. (4), where

$$\mathbf{A} = \begin{pmatrix} 1 & i\omega m_1 & 0 & 0 & 0 & 0 \\ -i\omega + \gamma_1 & m_1 \omega_1^2 & 0 & \hbar\lambda & -\hbar g c_s^* & -\hbar g c_s \\ 0 & 0 & 1 & i\omega m_2 & 0 & 0 \\ 0 & \hbar\lambda & -i\omega + \gamma_2 & m_2 \omega_2^2 & 0 & 0 \\ 0 & -i g c_s & 0 & 0 & \kappa + i(\Delta - \omega) & 0 \\ 0 & i g c_s^* & 0 & 0 & 0 & \kappa - i(\Delta + \omega) \end{pmatrix}, \quad (6)$$

and $\mathbf{B} = (0, \xi_1(\omega), 0, \xi_2(\omega), \sqrt{2\kappa}c_{in}(\omega), \sqrt{2\kappa}c_{in}^\dagger(-\omega))^T$. Thus the fluctuation $\delta c(\omega)$ of the cavity field can be solved by the linearized equations above.

Based on the input-output relation $c_{out}(\omega) = \sqrt{2\kappa}c(\omega) - c_{in}(\omega)$, we define the output field as $\tilde{c}_{out}(\omega) = c_{out}(\omega) + c_{in}(\omega) = \sqrt{2\kappa}c(\omega)$ in order to study the physical properties of the light field leaking out of the cavity, as in [17, 26]. Straightforward deduction yields

$$\begin{aligned} \delta \tilde{c}_{out}(\omega) &= E(\omega)c_{in}(\omega) + F(\omega)c_{in}^\dagger(-\omega) \\ &+ V_1(\omega)\xi_1(\omega) + V_2(\omega)\xi_2(\omega), \end{aligned} \quad (7)$$

where

$$\begin{aligned} E(\omega) &= 2\kappa \left[\frac{1}{\kappa + i(\Delta - \omega)} \right. \\ &\left. + \frac{i\hbar g^2 |c_s|^2 (\Delta + \omega + i\kappa) m_2 B_1}{(\Delta - \omega - i\kappa) d(\omega)} \right], \end{aligned} \quad (8)$$

$$\begin{aligned} F(\omega) &= \frac{-2i\kappa \hbar g^2 c_s^2 m_2 B_1}{d(\omega)}, \\ V_1(\omega) &= \frac{\sqrt{2\kappa} i c_s g [-\kappa + i(\Delta + \omega)] m_2 B_1}{d(\omega)}, \\ V_2(\omega) &= \frac{-\sqrt{2\kappa} \hbar g c_s \lambda (\Delta + \omega + i\kappa)}{d(\omega)}, \end{aligned} \quad (9)$$

with $d(\omega) = -\hbar^2 \lambda^2 A + m_2 B_1 (2|c_s|^2 g^2 \hbar \Delta + m_1 A B_2)$, $A = \Delta^2 + (\kappa - i\omega)^2$, $B_1 = \omega^2 + i\omega\gamma_2 - \omega_2^2$ and $B_2 = \omega^2 + i\omega\gamma_1 - \omega_1^2$.

Based on the above mentioned correlation functions of $c_{in}(\omega)$ and $\xi_\tau(\omega)$ as well as the standard homodyne detection [33] as plotted in Fig. 1, we may understand characteristics of the system from the homodyne spectrum $X(\omega)$, which can be analytically expressed as below provided that the fast oscillating terms at frequencies $\pm 2\omega_{1(2)}$ are omitted,

$$X(\omega) = E(\omega + \omega_1)E(-\omega + \omega_1) \frac{M\Gamma^2}{\Gamma^2 + \omega^2} + |E(\omega + \omega_1)|^2 \frac{N\Gamma^2}{\Gamma^2 + \omega^2}$$

$$\begin{aligned}
& + E^*(-\omega + \omega_1)E^*(\omega + \omega_1)\frac{M\Gamma^2}{\Gamma^2 + \omega^2} + |E(-\omega + \omega_1)|^2\frac{N\Gamma^2}{\Gamma^2 + \omega^2} \\
& + |E(\omega + \omega_1)|^2 + |F(-\omega + \omega_1)|^2 \\
& + |V_1(\omega + \omega_1)|^2\hbar\gamma_1m_1(\omega + \omega_1) \times \left\{ 1 + \coth\left[\frac{\hbar(\omega + \omega_1)}{2k_B T}\right] \right\} \\
& + |V_2(\omega + \omega_1)|^2\hbar\gamma_2m_2(\omega + \omega_1) \times \left\{ 1 + \coth\left[\frac{\hbar(\omega + \omega_1)}{2k_B T}\right] \right\} \\
& + |V_1(-\omega + \omega_1)|^2\hbar\gamma_1m_1(\omega - \omega_1) \times \left\{ 1 + \coth\left[\frac{\hbar(\omega - \omega_1)}{2k_B T}\right] \right\} \\
& + |V_2(-\omega + \omega_1)|^2\hbar\gamma_2m_2(\omega - \omega_1) \times \left\{ 1 + \coth\left[\frac{\hbar(\omega - \omega_1)}{2k_B T}\right] \right\}, \tag{10}
\end{aligned}$$

where the first four terms are from the input squeezed field and the next two terms are relevant to the spontaneous emission of the input vacuum noise. The rest terms are caused by the thermal noise of the NAMRs, which is temperature dependent. So the squeezed field employed does not work better for the temperature-dependent effects in comparison to other quantum fields, but enhancing the measurement precision in the homodyne spectrum. In addition, Eq. (10) is more general with respect to the counterpart in Ref. [26], since it can be reduced to Eq. (13) in [26] if $\lambda = 0$, i.e., in the absence of the Coulomb coupling.

III. HOMODYNE SPECTRA OF THE DOUBLE OMIT

We specify below some unique characteristics of the double OMIT by the numerically calculated homodyne spectra. For simplicity, we first suppose the two NAMRs to be identical in our treatment. The non-identical case, which is more general but not fundamentally different, will be justified later.

Our numerical calculation is carried out based on realistic parameter values [34]. We consider an optomechanical cavity with length $L = 25$ mm and decay rate $\kappa \sim 2\pi \times 215$ kHz, driven by the pump field of wavelength $\lambda_l = 2\pi c/\omega_l = 1064$ nm. For the two identical NAMRs, we assume the effective mass $m_1 = m_2 = 145$ ng, the eigen-frequencies $\omega_m = \omega_1 = \omega_2 = 2\pi \times 947$ kHz, the decay rates $\gamma_m = \gamma_1 = \gamma_2 = 2\pi \times 141$ Hz, and the quality factors $Q_1 = Q_2 = \omega_m/\gamma_m = 6700$. In addition, the linewidth of the squeezed vacuum is supposed to be $\Gamma = 2\kappa$.

In most of the calculations below, we employ the zero temperature $T = 0$ and the photon number $N = 5$ in the squeezed vacuum, and assume the coupling field power $\wp = 2$ mW and the coupling strength unit $\lambda_0 = 4 \times 10^{36}$ Hz/m². The homodyne spectrum $X(\omega)$ plotted in Fig. 2(a) presents the change from a single transparency window to two transparency windows with increasing Coulomb coupling, which reflects a fact that the

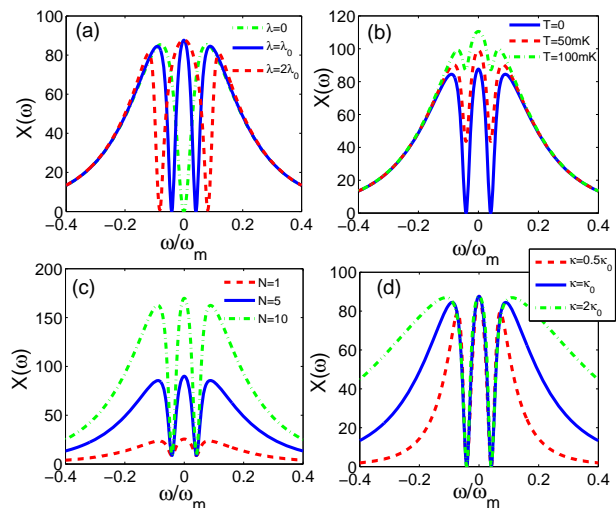


FIG. 2: (Color online) The homodyne spectra $X(\omega)$ of the output field as functions of the normalized frequency ω/ω_m , where (a) for different Coulomb coupling λ with the coupling strength unit $\lambda_0 = 4 \times 10^{36}$ Hz/m²; (b) for different temperature T with $N=5$; (c) for different photon number N with $T = 10$ mK; (d) for different cavity decay κ with the decay unit $\kappa_0 = 2\pi \times 215$ kHz.

Coulomb coupling breaks down the original interference in the OMIT and splits the bosonic mode of the system into two. Since the energy difference between the two split bosonic modes depends on the Coulomb coupling, the splitting of the transparency windows is relevant to the Coulomb coupling [23]. However, the middle peak is fixed no matter how much the Coulomb coupling varies.

For a finite temperature, the homodyne spectrum $X(\omega)$ still works for the double OMIT, as presented in Fig. 2(b) where the visible middle peak and two nadirs exist even at $T = 100$ mK. However, the trend reflected in Fig. 2(b) indicates that the double-OMIT will definitely disappear with further increase of the temperature. Besides, a more careful calculation shows that the photon number plays an important role in the $X(\omega)$ variation. From Fig. 2(c), we find that the middle peak and two

nadirs are visible at $T = 10$ mK, even for the squeezed state at the single-photon level (the red dashed curve). In particular, compared with Fig. 2(b), we find that the two nadirs of the double OMIT are fixed with the variation of the photon number, but changing with the temperature.

Moreover, the cavity decay modifies the profiles of the transparency windows, as plotted in Fig. 2(d). However, although the profiles become narrower and sharper with smaller cavity decay rate κ , the peak and the nadirs of the two transparency windows remain unchanged, implying robustness against the cavity decay at these points.

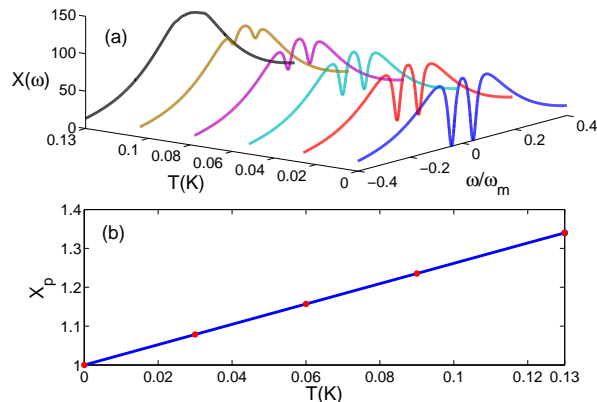


FIG. 3: (Color online) (a) The homodyne spectra $X(\omega)$ as functions of the frequency ω/ω_m and the temperature T for $\lambda = \lambda_0$. (b) The rescaled middle peak value X_p (in units of $X_0 = 87.59$) as a function of the temperature T for $\lambda = \lambda_0$, where the temperature measurement is available within the range $0 \leq T \leq 0.13$ K. The upper limit of the measured temperature is restricted by the measurement resolution 1% of X_p at $T = 0.13$ K. Other parameters take the same values as in Fig. 2(a).

IV. MEASUREMENT OF THE ENVIRONMENTAL TEMPERATURE

Using above indicated properties of the homodyne spectrum $X(\omega)$, we may carry out precision measurement of the environmental temperature using the double-OMIT with the squeeze field.

Fig. 3(a) presents the step-by-step change of $X(\omega)$ with the environmental temperature, where the middle peak increases linearly with the temperature. Since we have renormalized the middle peak value by $X_p = X(0)/X_0$ with $X_0 = 87.59 = X(0)$ at zero temperature, the temperature change can be exactly known from Fig. 3(b) by precisely measuring the variation of X_p . But as shown in Fig. 3(a), the height difference between the middle peak and the two nadirs shrinks with the tem-

perature increasing. This implies an upper limit of the

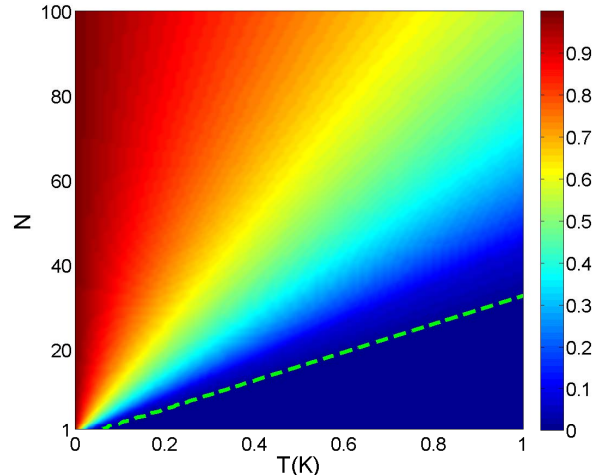


FIG. 4: (Color online) The quantum signal visibility (QSV) as functions of the photon number N and temperature T for $\lambda = \lambda_0$. The dashed line in green represents a borderline for available measurement, below which QSV is less than the measurement resolution 1%. Other parameters are of the same values as in Fig. 2(a).

measured temperature, e.g., $T = 0.13$ K where the double OMIT reaches the resolution limit of the observation.

Specifically, for the linear variation of X_p with respect to T in Fig. 3(b), the sensitivity can be evaluated by the slope $k = \partial T / \partial X(0) = 4.4 \times 10^{-3}$ K. As a result, for a measurement resolution $\delta X(0) = 1\%$ of the peak value, the detectable temperature change can be minimized to 4.4×10^{-5} K, which is lower by one order of magnitude compared to a quantum thermometer designed based on a noise measurement using the electron charge [35]. The linear variation of the middle peak with respect to the temperature can be understood from Eq. (10) in which the last four terms are reduced to be linearly changing with T if $T \rightarrow 0$. In fact, the measurement precision in our case can be further enhanced if we elaborately change the mass ratio of the two NAMRs, as discussed later. We have to emphasize that this measurement based on the peak values is insensitive to the change of Coulomb coupling, as indicated in Fig. 2(a).

To carry out a precision measurement in our scheme, we have to have a big enough contrast of $X(\omega)$ for our observation. To this end, we consider below the influence from the photon number and the environmental temperature. When the two NAMRs are identical, if many photons are involved in the squeezed state, we have $N \approx M$, and Eq. (10) at low temperature ($T \rightarrow 0$) expands to the first order at the frequency of the peak point ($\omega_{peak} \equiv 0$) as

$$\begin{aligned}
X(\omega_{peak}) = X(0) &= N[E(\omega_m) + E^*(\omega_m)]^2 + |E(\omega_m)|^2 + |F(\omega_m)|^2 \\
&+ 2|V_1(\omega_m)|^2 \hbar \gamma_1 m_1 \omega_m \coth\left[\frac{\hbar \omega_m}{2k_B T}\right] \\
&+ 2|V_2(\omega_m)|^2 \hbar \gamma_2 m_2 \omega_m \coth\left[\frac{\hbar \omega_m}{2k_B T}\right] \\
&= N[E(\omega_m) + E^*(\omega_m)]^2 + |E(\omega_m)|^2 + |F(\omega_m)|^2 + k(0)T,
\end{aligned} \tag{11}$$

where the slope is $k(0) = 4k_B \gamma_m m [|V_1(\omega_m)|^2 + |V_2(\omega_m)|^2]$, N is relevant to the quantum signal terms which compete with the last two thermal noise terms involving T . With the increase of T , the values of the thermal noise terms will exceed those of the quantum signal terms and thus the quantum signal is completely buried by the thermal noise, i.e., disappearance of the double OMIT. To clarify this point, we define quantum signal visibility $QSV = (\text{peak} - \text{nadir})/\text{peak}$ as a contrast of our observation, where $QSV = 1$ implies an overwhelming quantum signal and disappearance of the double OMIT corresponds to $QSV = 0$. Involvement of more photons helps increasing the contrast, as indicated in Fig. 2(c) and understood from Eq. (11). We plot in Fig. 4 a borderline for available precision measurement, below which QSV is smaller than 1%, the measurement resolution we assumed above. As such, if $T = 0$, the double OMIT always exists no matter how many photons are involved. But with T increasing, more photons are required to be involved if our proposed measurement of the environmental temperature works.

V. DISCUSSION

The precision measurement of the environmental temperature described above is based on identical NAMRs. A more general and realistic case is with non-identical NAMRs, which are different in frequency or mass. In such cases, our model has different characteristics and thus different applications.

As an example, we first consider in Fig. 5 the situation with different frequencies of the two NAMRs. In this case, the profile of the double OMIT keeps changing with the frequency difference $\Delta\omega = |\omega_1 - \omega_2|$, where the double windows are first split into triple windows and then become a standard OMIT with a single window, like the absence of Coulomb coupling (See Fig. 5(a)). Fig. 5(b) provides another view angle to observe the role played by the Coulomb coupling. Different from the situation with identical NAMRs, the Coulomb coupling yields triple windows directly from the single window once the Coulomb coupling turns to be non-zero. This feature is actually resulted by the interference of two double OMITs with two asymmetric windows due to the frequency difference. As indicated by the homodyne spectra in Figs. 5(a) and 5(b), although the profiles

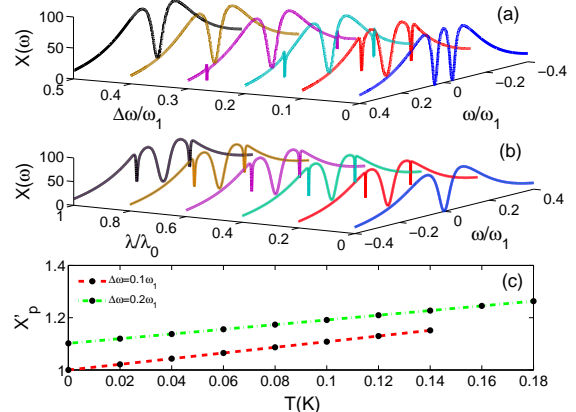


FIG. 5: (Color online) (a) The homodyne spectra $X(\omega)$ as functions of ω/ω_1 and $\Delta\omega/\omega_1$ for $\lambda = \lambda_0$. (b) The homodyne spectra $X(\omega)$ as functions of ω/ω_1 and λ/λ_0 with $\Delta\omega = 0.1\omega_1$. (c) The rescaled peak value X'_p (in units of 84.03) as a function of the temperature T for $\lambda = \lambda_0$, where the available measurement of the temperature is $0 \leq T \leq 0.14$ K ($\Delta\omega = 0.1\omega_1$) or $0 \leq T \leq 0.18$ K ($\Delta\omega = 0.2\omega_1$). The upper limit of the measured temperature is restricted by the measurement resolution 1% of X'_p . Other parameters are of the same values as in Fig. 2(a).

of the spectra change in the variation of $\Delta\omega$ and λ , the two symmetric peaks in the case of triple windows are always fixed, where the two peak values can be evaluated by $\frac{\partial X(\omega)}{\partial \omega}|_{\omega=\omega_{\pm}} = 0$ and $\frac{\partial^2 X(\omega)}{\partial^2 \omega}|_{\omega=\omega_{\pm}} < 0$, with ω_{\pm} the frequencies relevant to the two symmetric peaks.

Based on this feature, we consider below a measurement of the environmental temperature using one of the peak values (See Fig. 5(c)). The peak value varies linearly with respect to T , in the same fashion as in Fig. 3(b) for the middle peak values in the case of identical NAMRs. We may find a similar formula to Eq. (11) for the slope of the peak values $X(\omega_{peak})$ varying with the environmental temperature T as

$$\begin{aligned}
k(\omega_{peak}) &= 2k_B \sum_{j=1}^2 \gamma_j m_j [|V_j(\omega_{peak} + \omega_1)|^2 \\
&+ |V_j(-\omega_{peak} + \omega_1)|^2] = k(-\omega_{peak}).
\end{aligned} \tag{12}$$

Straightforward calculations of the slopes in this case

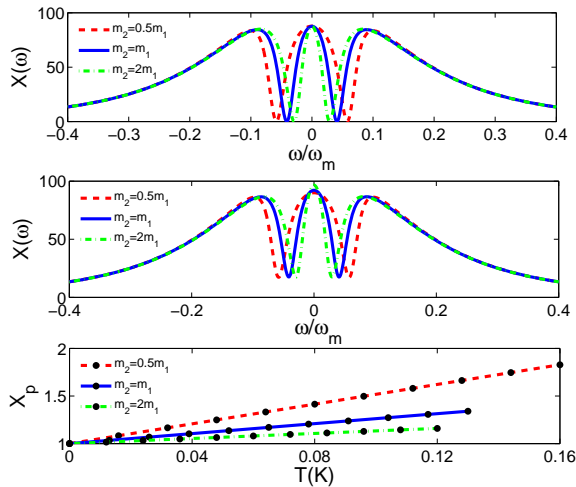


FIG. 6: (Color online) (a) The homodyne spectra $X(\omega)$ as functions of ω/ω_m for $\lambda = \lambda_0$ and $T=0$. (b) The homodyne spectra $X(\omega)$ as functions of ω/ω_m for $\lambda = \lambda_0$ and $T = 20$ mK. (c) The rescaled middle peak value X_p (in units of 87.59) as a function of the temperature T for $\lambda = \lambda_0$, where the temperature measurement is available within the range $0 \leq T \leq 0.16$ K ($m_2 = 0.5m_1$) or $0 \leq T \leq 0.12$ K ($m_2 = 2m_1$). The upper limit of the measured temperature is restricted by the measurement resolution 1% of X_p . Other parameters take the same values as in Fig. 2(a).

present less precise measurements of the environmental temperature compared to the case of identical NAMRs since we have the sensitivity with 0.44 ($\Delta\omega = 0.1\omega_1$) or 0.33 ($\Delta\omega = 0.2\omega_1$) of the counterpart in the case of $\Delta\omega = 0$. Therefore, for a more precise measurement of the environmental temperature with two different NAMRs, the frequency difference is required to be as tiny as possible.

If the two different NAMRs are with the same frequency but with different mass, we have only double OMITs, rather than triple OMITs. In this case, we found that the middle peak remains the same value for different ratios of m_2/m_1 provided that the temperature is zero, but varies with different slopes for different ratios of m_2/m_1 if $T \neq 0$ (See Fig. 6). In particular, for a bigger mass of NAMR₂ than NAMR₁, e.g., $m_2 = 2m_1$ in Fig. 6(c), the measurement sensitivity of the environmental temperature is higher than the counterpart in the iden-

tical case. In addition, the measurement range changes with different ratios of m_2/m_1 as indicated in Fig. 6(c). Nevertheless, within the range $T \in [0, 0.12]$ K, we have the possibility to obtain the measurement precision of temperature better than 4.4×10^{-5} K.

VI. CONCLUSION

In summary, we have justified the possibility of precisely detecting the environmental temperature by the unique quantum characteristics of double-OMIT. To our knowledge, this is the first scheme for such a precision measurement in the optomechanical system via the noise spectra. We have shown by numerical simulation that we are able to have a better precision of measuring the environmental temperature than a previously reported quantum thermometer [35].

For simplicity, however, we have remained the radiation pressure as a constant throughout the paper. For a thorough investigation of the temperature measurement, it is necessary to explore the change of the radiation pressure. Straightforward calculations indicate that enhancement of the radiation pressure due to increase of the photon number will definitely lead to a better precision measurement of the environmental temperature. Nevertheless, the nonlinear effect in the optomechanics due to more photons involved would bring in unexpected complexity, which needs further scrutiny.

Moreover, due to the tunable fashion and robustness to cavity decay, the model under consideration can also be applied to other applications, such as precisely measuring Coulomb coupling strength and the frequency (mass) difference between the two NAMRs. Further exploration would be more interesting and is underway.

Acknowledgments

This work is supported by the National Natural Science Foundation of China under Grants No. 61475045, No. 11274352 and No. 11304366, the China Postdoctoral Science Foundation (Grants No. 2013M531771 and No. 2014T70760), and Natural Science Funding for Colleges and Universities in Jiangsu Province (Grant No. 12KJD140002).

[1] M. Fleischhauer, A. Imamoglu, and J. P. Marangos, *Rev. Mod. Phys.* **77**, 633 (2005).
 [2] H.-Y. Lo, P.-C. Su, and Y.-F. Chen, *Phys. Rev. A* **81**, 053829 (2010).
 [3] J. Q. Shen and S. He, *Phys. Rev. A* **74**, 063831 (2006).
 [4] L. V. Hau, S. E. Harris, Z. Dutton, and C. H. Behroozi, *Nature (London)* **397**, 594 (1999).
 [5] A. I. Lvovsky, B. C. Sanders, and W. Tittel, *Nat. Photonics* **3**, 706 (2009).

[6] I. Novikova, R. Walsworth, and Y. Xiao, *Laser Photonics Rev.* **6**, 333 (2012).
 [7] V. M. Acosta, K. Jensen, C. Santori, D. Budker, and R. G. Beausoleil, *Phys. Rev. Lett.* **110**, 213605 (2013).
 [8] J. Q. Shen, *Phys. Rev. A* **90**, 023814 (2014).
 [9] J. Q. Zhang, S. Zhang, J. H. Zou, L. Chen, W. Yang, Y. Li, and M. Feng, *Opt. Express* **21**, 29695 (2013).
 [10] Y. Chang and C. P. Sun, *Phys. Rev. A* **83**, 053834 (2011).
 [11] X. Q. Luo, D. L. Wang, Z. Q. Zhang, J. W. Ding, and

- W. M. Liu, Phys. Rev. A **84**, 033803 (2011).
- [12] J. Cheng and G. Huang, Phys. Rev. A **83**, 053847 (2011).
- [13] K.-P. Marzlin, Jürgen Appel, and A. I. Lvovsky, Phys. Rev. A **77**, 043813 (2008).
- [14] S. Weis, R. Rivière, S. Deléglise, E. Gavartin, O. Arcizet, A. Schliesser, and T. J. Kippenberg, Science **330**, 1520 (2010).
- [15] G. S. Agarwal and S. Huang, Phys. Rev. A **81**, 041803 (2010).
- [16] S. Huang and G. S. Agarwal, Phys. Rev. A **83**, 023823 (2011).
- [17] H. Xiong, L.-G. Si, A.-S. Zheng, X. Yang, and Y. Wu, Phys. Rev. A **86**, 013815 (2012).
- [18] Q. Lin, J. Rosenberg, D. Chang, R. Camacho, M. Eichenfield, K. J. Vahala, and O. Painter, Nat. Photon. **4**, 236 (2010).
- [19] J. D. Teufel, D. Li, M. S. Allman, K. Cicak, A. J. Sirois, J. D. Whittaker, and R. W. Simmonds, Nature (London) **471**, 204 (2011).
- [20] A. H. Safavi-Naeini, T. P. Mayer Alegre, J. Chan, M. Eichenfield, M. Winger, Q. Lin, J. T. Hill, D. Chang, and O. Painter, Nature (London) **472**, 69 (2011).
- [21] J. Q. Zhang, Y. Li, M. Feng, and Y. Xu, Phys. Rev. A **86**, 053806 (2012).
- [22] S. Shahidani, M. H. Naderi, and M. Soltanolkotabi, Phys. Rev. A **88**, 053813 (2013).
- [23] H. Wang, X. Gu, Y.-X. Liu, A. Miranowicz, and Franco Nori, Phys. Rev. A **90**, 023817 (2014).
- [24] P. C. Ma, J. Q. Zhang, Y. Xiao, M. Feng, and Z. M. Zhang, Phys. Rev. A **90**, 043825 (2014).
- [25] S. Huang, J. Phys. B **47**, 055504 (2014).
- [26] S. Huang and G. S. Agarwal, Phys. Rev. A **83**, 043826 (2011).
- [27] C. Benedetti, F. Buscemi, P. Bordone, and M. G. A. Paris, Phys. Rev. A **89**, 032114 (2014).
- [28] M. Karuza, C. Biancofiore, M. Bawaj, C. Molinelli, M. Galassi, R. Natali, P. Tombesi, G. Di Giuseppe, and D. Vitali, Phys. Rev. A **88**, 013804 (2013).
- [29] G. Goldstein, P. Cappellaro, J. R. Maze, J. S. Hodges, L. Jiang, A. S. Sørensen, and M. D. Lukin, Phys. Rev. Lett. **106**, 140502 (2011).
- [30] G. Strübi and C. Bruder, Phys. Rev. Lett. **110**, 083605 (2013).
- [31] W. K. Hensinger, D. W. Utami, H. S. Goan, K. Schwab, C. Monroe, and G. J. Milburn, Phys. Rev. A **72**, 041405(R) (2005).
- [32] L. Tian and P. Zoller, Phys. Rev. Lett. **93**, 266403 (2004).
- [33] C. C. Gerry and P. L. Knight, *Introductory Quantum Optics* (Cambridge University Press, New York, 2005).
- [34] S. Gröblacher, K. Hammerer, M. R. Vanner, and M. Aspelmeyer, Nature (London) **460**, 724 (2009).
- [35] L. Spietz, K. W. Lehnert, I. Siddiqi, and R. J. Schoelkopf, Science **300**, 1929 (2003).